CERN – EUROPEAN ORGANIZATION FOR NUCLEAR RESEARCH

CLIC – Note – 1082

# RF DESIGN OF ACCELERATING STRUCTURE FOR THE MAIN LINAC OF THE KLYSTRON-BASED FIRST STAGE OF CLIC AT 380 GEV

Jiayang Liu[1,2], Alexej Grudiev[2]

[1]Tsinghua University, Beijing, China
[2]CERN, Geneva, Switzerland

CERN-ACC-2018-0034
12/10/2018

**Abstract**

An alternative klystron-based scenario for the first stage of Compact Linear Collider (CLIC) at 380 GeV center-of-mass energy was proposed. Compared to the two-beam scheme, klystron-based one is easily tested and implemented, and is expected to reduce the cost of the first stage at 380 GeV. The RF design and parameters of the klystron-based accelerating structure named CLIC-K are described in this paper. The optimization of the high-order-mode (HOM) damping loads used to suppress the long-range transverse wakefield is also presented.

Geneva, Switzerland
12 October 2018

**RF design of accelerating structure for the main linac of the klystron-based first stage of CLIC at 380 GeV**

Jiayang Liu (1,2), Alexej Grudiev (2)

(1) Tsinghua University, Beijing, China

(2) CERN, Geneva, Switzerland

**Abstract**

An alternative klystron-based scenario for the first stage of Compact Linear Collider (CLIC) at 380 GeV center-of-mass energy was proposed. Compared to the two-beam scheme, klystron-based one is easily tested and implemented, and is expected to reduce the cost of the first stage at 380 GeV. The RF design and parameters of the klystron-based accelerating structure named CLIC-K are described in this paper. The optimization of the high-order-mode (HOM) damping loads used to suppress the long-range transverse wakefield is also presented.

**I. Introduction**

It is generally agreed that high center-of-mass energy collider is the most powerful tool for the development and research of high energy physics [1,2]. CLIC [3] is one of the candidates. A novel design of two-beam scheme was fully optimized for 3 TeV stage to save the cost on RF power sources and make the number of L-band klystrons at a manageable value. The high peak current of the drive beam is at a large value of 100 A. Power Extraction and Transfer Structures (PETS) are used to extract the power from the drive beam to the main beam. However, this system is relatively expensive at low energy.

The baseline for a staged CLIC was updated in 2016 [4]. An alternative scenario for the first stage at 380 GeV using X-band klystrons was proposed. Compared to the two-beam scheme, klystron-based one is expected to be competitive in cost at lower energy, which is illustrated in Figure 1. Moreover, with the ongoing developments of the modulators and high-efficiency klystrons [5,6], the interest of klystron-based scenario will be more considerable. Another advantage of the klystron-based option is that the full RF system is similar with the high-power test setup so that it can be tested more easily and be implemented faster [7].

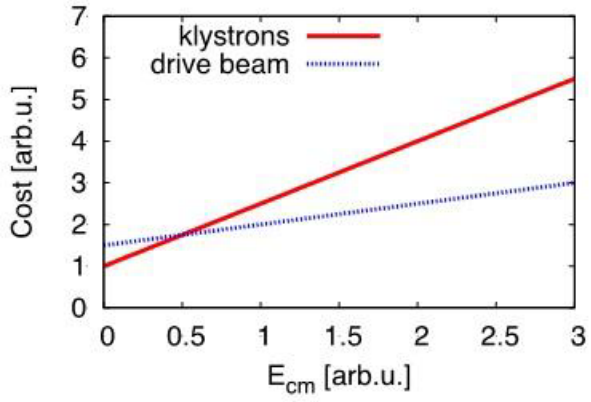


Figure 1. A comparison of cost between klystron-based and two-beam linear collider.

A conceptual design of the RF unit for klystron-based CLIC has been developed [8], as shown in Figure 2. It consists of two X-band klystrons, a correction cavity chain, two SLAC Energy Doubler X-band pulse compressors (SLEDXs), eight accelerating structures and some RF components. The RF power produced by two klystrons are combined in a 3-dB hybrid and the pulse shape is modified by the following correction cavity chain [9]. Then, the long RF pulse is compressed into short one with higher peak RF power by SLEDXs and split into eight accelerating structures. The accelerator parameters at 380 GeV has been optimized to minimize the cost [4]. The cheapest klystron-based accelerating structure

design was named CLIC-K. Compared with the 3 TeV baseline CLIC-G design [3], the irises of CLIC-K have a larger average radius and taper more heavily. The expected average loaded accelerating gradient of 75 MV/m is lower than for 3 TeV, as described in Table 1.

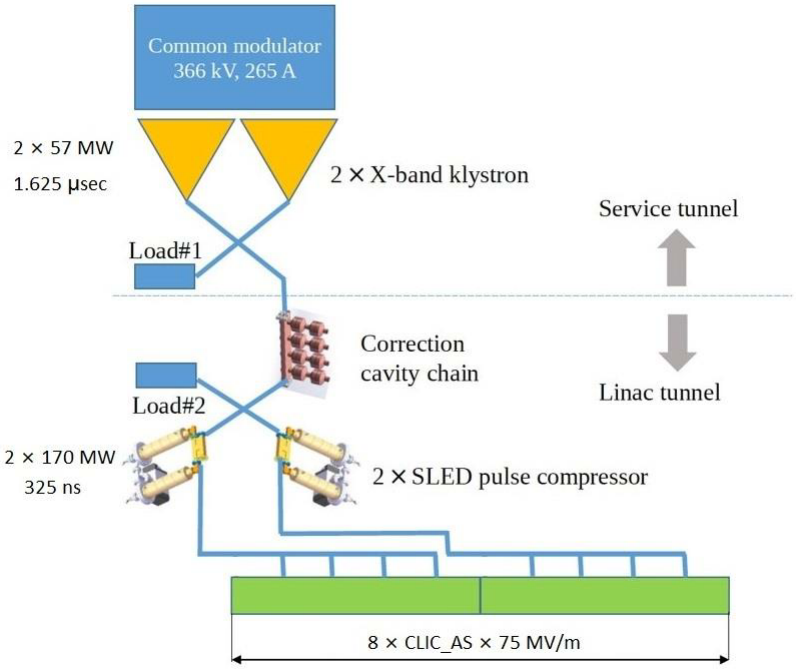


Figure 2. Conceptual design of the RF unit for klystron-based CLIC.

Table 1. Comparison between CLIC-G and CLIC-K

| Parameters | CLIC-G | CLIC-K |
|---|---|---|
| Frequency | 11.994 GHz | 11.994 GHz |
| Accelerating gradient | 100 MV/m | 75 MV/m |
| Active length | 0.23 m | 0.23 m |
| RF phase advance per cell | 120 ° | 120 ° |
| Number of cells | 28 | 28 |
| Average iris radius / RF wavelength | 0.11 | 0.1175 |
| First iris radius / RF wavelength | 0.126 | 0.145 |
| Last iris radius / RF wavelength | 0.094 | 0.09 |
| First iris thickness / cell length | 0.2 | 0.25 |
| Last iris thickness / cell length | 0.12 | 0.134 |
| Bunch spacing | 0.15 m | 0.15 m |
| Number of particles per bunch | $3.72\times10^{9}$ | $3.87\times10^{9}$ |
| Number of bunches per train | 312 | 485 |

In the past decade, a number of CLIC accelerator prototypes have been designed, fabricated and tested [10-18], as summarized in Figure 3. The gradients achieved in the structures with damping features were generally 80% to 90% lower than those of undamped structures. Nevertheless, to preserve the stability and luminosity of beams in CLIC, the long-range transverse wakefield in main linac must be suppressed to an acceptable value [19]. The method adopt in the baseline design for CLIC main linac is waveguide damping [20,21]. The regular cell geometry of the CLIC main linac is shown in Figure 4. Four waveguides are coupled to the accelerating cell to damp the HOMs excited in the main linac. The design of the accelerating structure CLIC-K is also based on the waveguide damping structure.

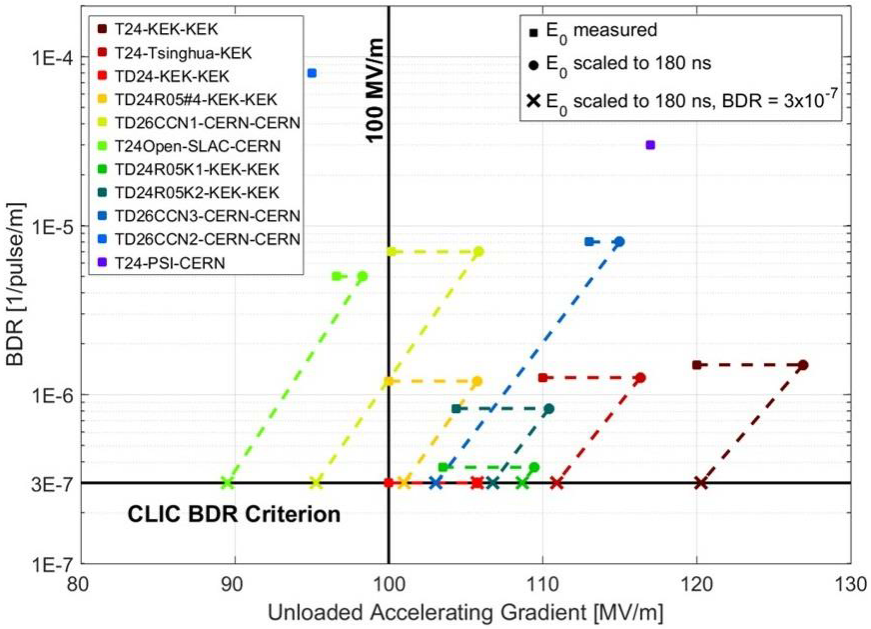


Figure 3. Results of high-power tests on the CLIC accelerating structure prototypes.

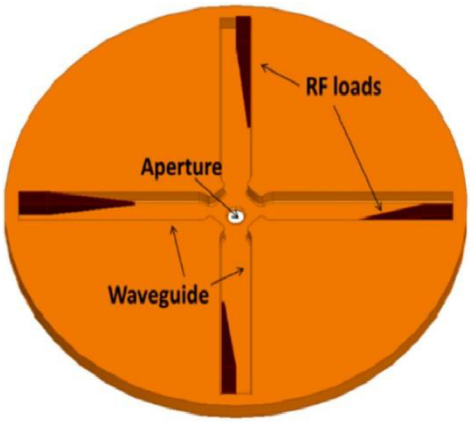


Figure 4. Regular cell geometry of CLIC main linac.

In this paper, the details of RF design and parameters of the accelerating structure CLIC-K based on HFSS code [22] are described in Sec. II. The results of wakefield suppression and the design of HOM loads are introduced in Sec. III. The simulations of wakefield excited in accelerating structure is carried out by GdfidL code [23]. The accuracy of the code has been verified in the previous experiment [24].

## II. Accelerating structure design

### II.1 Design of the regular cells

In high-gradient accelerating structures, the limitation of performance is due to vacuum RF breakdown. It is a complicated phenomenon that can be predicted by the maximum of surface electric field, surface RF pulsed heating and the modified Poynting vector $S_c$ [25-26]. To minimize the surface electric field and $S_c$, the optimization of iris shape was conducted by using HFSS. As for the RF pulsed heating, a fourth-order polynomial curve with smoother curvature change was proposed and replaced the elliptical curve to minimize the surface magnetic field on the outer wall of the cell [14]. The results of the single cell design in the accelerating structure CLIC-K are illustrated in Figure 5.

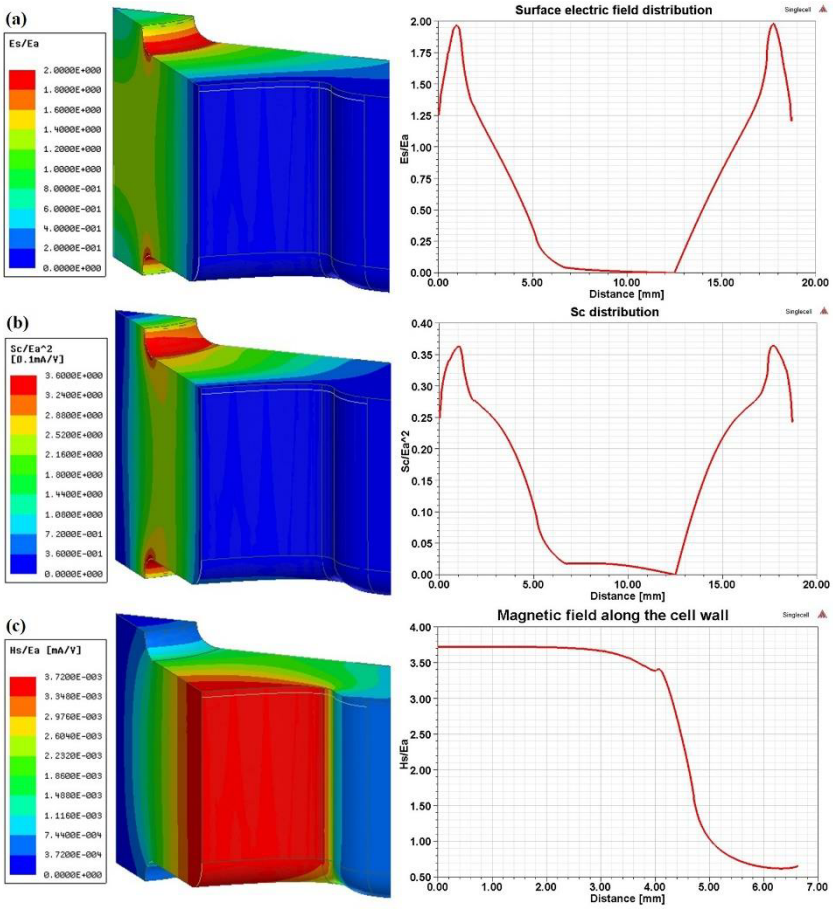


Figure 5. (a) Electric field distribution, (b) $S_c$ distribution and (c) magnetic field distribution on the surface of the middle cell (1/8 view)

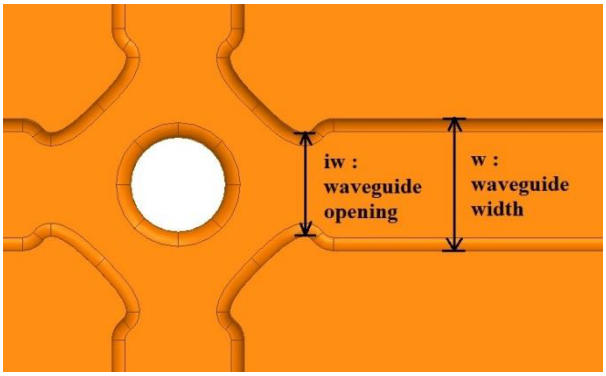


Figure 6. Geometrical parameters defined in cells.

Moreover, the design of the damping waveguide structure was optimized. The related parameters are shown in Figure 6. The width of the waveguide was selected as 10.1 mm, which has been analyzed in the optimization of baseline CLIC-G design [14]. The dimension of the waveguide opening, named “iw”, has significant impact on the wakefield suppression, pulsed surface heating temperature rise and RF-to-beam efficiency. A larger waveguide opening results in a stronger wakefield suppression but a higher surface magnetic field, a lower Q-factor and a lower shunt impedance, which means a higher pulsed surface heating temperature rise and a lower RF-to-beam efficiency. A trade-off needs to be made in the optimization of waveguide opening. The simulations of wakefield suppression and RF parameters were carried out by GdfidL and HFSS, as shown in Figure 7. The final dimension of the waveguide opening is tapered from 7.9 mm to 7.7 mm.

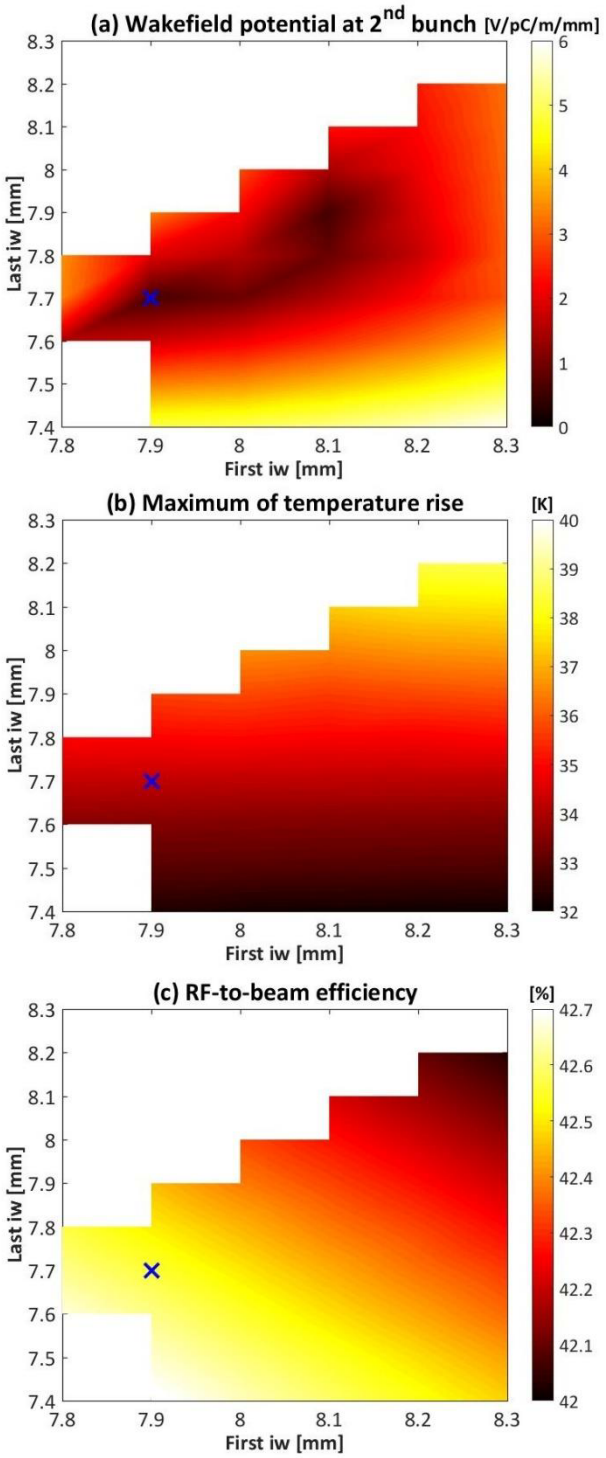


Figure 7. (a) Wakefield potential at second bunch, (b) maximum of temperature rise in the structure and (c) RF-to-beam efficiency distribution with different linear tapering on waveguide opening. The spot "×" indicates the parameters selected in the CLIC-K.

Table 2. RF parameters of the first, middle and last cells.

| RF parameters | First cell | Middle cell | Last cell |
|---|---|---|---|
| Q-factor (Cu) | 5619 | 5786 | 5962 |
| Group velocity [% of c] | 2.362 | 1.370 | 0.682 |
| Shunt impedance [MΩ/m] | 73 | 91 | 112 |

| | | | |
|---|---|---|---|
| $E_{surf}$ / $E_{acc}$ | 2.04 | 2.00 | 1.97 |
| $H_{surf}$ / $E_{acc}$ [mA/V] | 4.15 | 3.72 | 3.34 |
| $S_c$ / $E_{acc}^2$ [mA/V] | 0.49 | 0.36 | 0.26 |

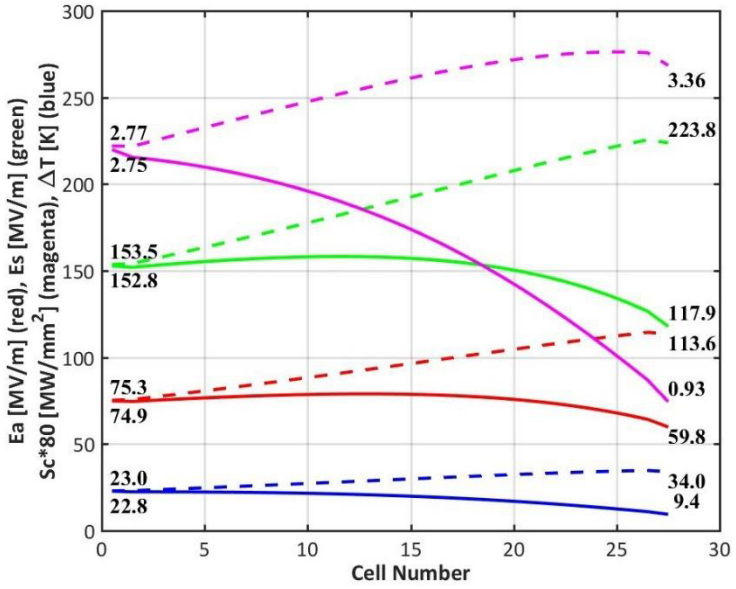


Figure 8. Distribution of RF parameters for loaded (solid) and unloaded (dashed) conditions.

The RF parameters of the first, middle and last cells are summarized in Table 2. The distribution of these parameters in the accelerating structure CLIC-K calculated analytically based on the interpolation of the first middle and last cells parameters is presented in Figure 8.

**II.2 Coupler design**

The input and output coupler cells were designed in a similar way as the compact couplers for CLIC-G. The length of the coupler cells was kept same as in the baseline design: 6.66 mm. The width of input and output waveguides is 22.86 mm (WR90 width). The radius and waveguide opening were optimized to match the WR90 waveguides and the accelerating structure. The match of the output coupler cell was based on the analysis of the amplitude of forward and backward waves, as expressed in the Equation (1).

$$\left.\begin{aligned} E_1 &= ae^{-j\varphi} + be^{j\varphi} \\ E_2 &= a + b \\ E_3 &= ae^{j\varphi} + be^{-j\varphi} \end{aligned}\right\} \Rightarrow \frac{b}{a} = \frac{\sqrt{u^2-4}-v}{\sqrt{u^2-4}+v}, u = \frac{E_3+E_1}{E_2}, v = \frac{E_3-E_1}{E_2} \quad (1)$$

Where $E_1$, $E_2$, $E_3$ are the peak electric field of last three cells, φ is the phase advance (2/3π) between two cells, a and b are the amplitudes of the forward and backward waves, as shown in Figure 9. The match of the input coupler cell was done by minimizing $S_{11}$.

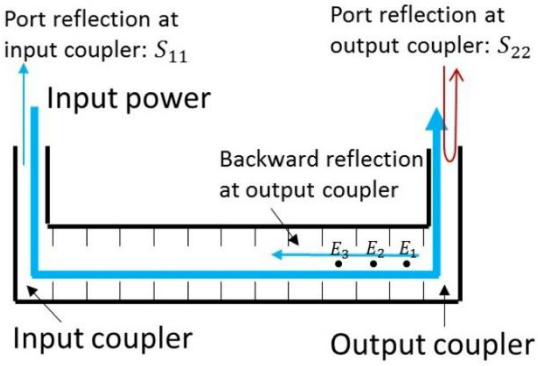

Figure 9. Reflection defined in the travelling wave structure.

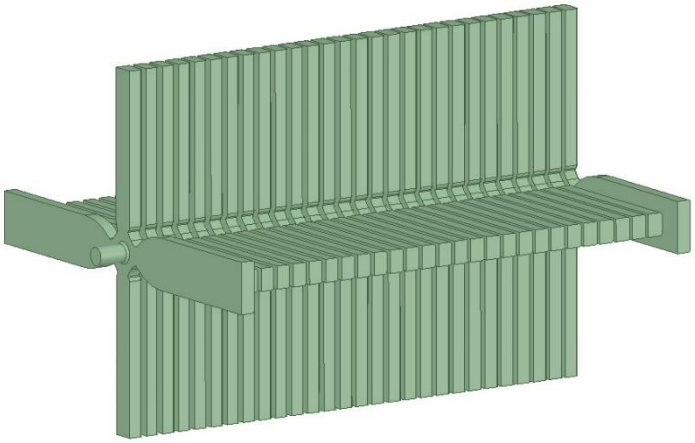

Figure 10. Vacuum volume of the full tapered structure.

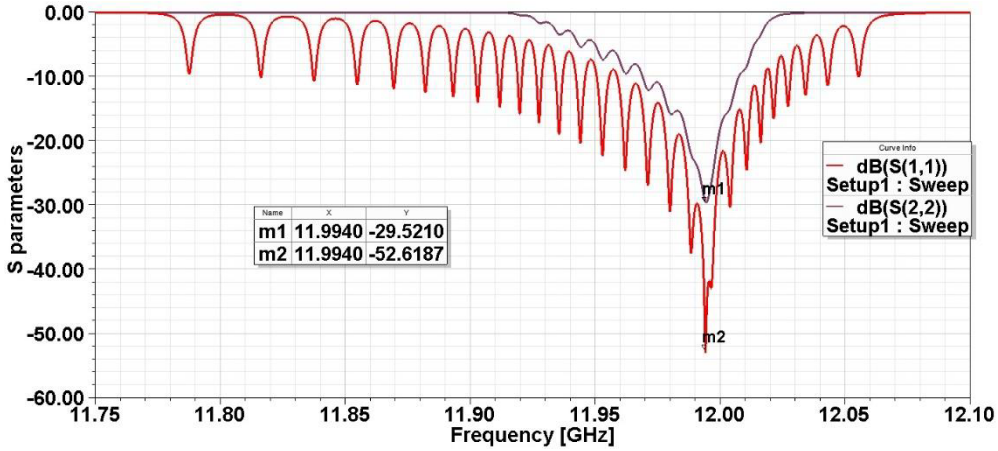


Figure 11. Reflections of the accelerating structure CLIC-K.

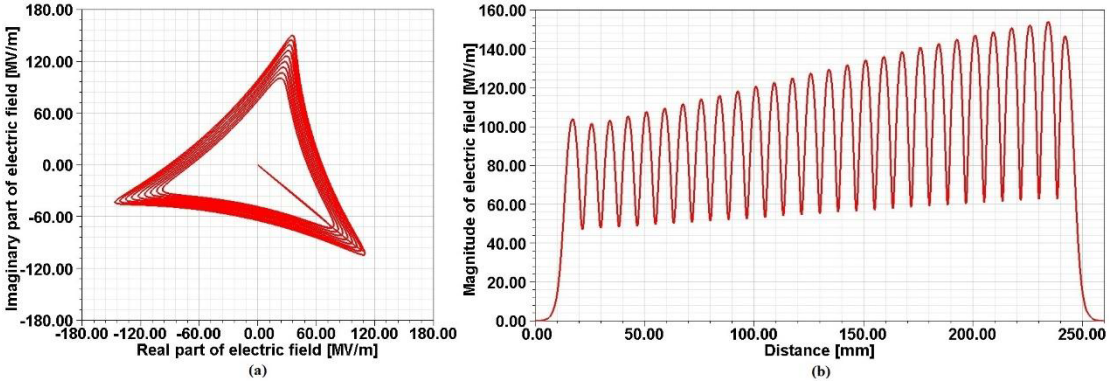


Figure 12. Electric field distribution along the beam path. (a) Complex electric field. (b) Magnitude of electric field.

The full tapered structure includes 26 regular cells and 2 coupler cells, as shown in Figure 10. The reflection at the input coupler was optimized below -50 dB, as illustrated in Figure 11. The distribution of electric field along the beam path is presented in Figure 12. From this field distribution, the backward reflection b/a calculated by the amplitude of forward and backward waves along the full structure was conducted and presented in Figure 13. The reflections in the regular cells are below -50 dB. The rapid declining and rising of the slope at the beginning and end are caused by the differences between coupler cells and regular cells.

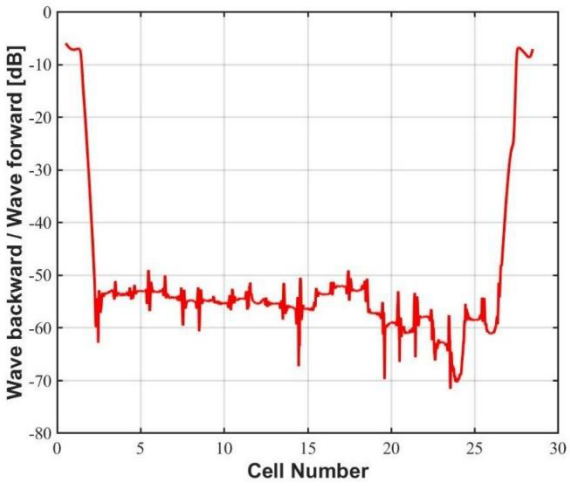


Figure 13. The local reflection along the full accelerating structure.

The RF parameters of the accelerating structure CLIC-K are described in Table 3. Due to the limited structure bandwidth and for beam-loading compensation purposes, two ramps during the rise time $\tau_r$ and filling time $\tau_f$ are necessary in the input pulse [27,28], respectively. The rise time is scaled from the $\tau_r$ of the CLIC-G, as expressed in the Equation (2). The filling time is calculated from the distribution of $S_{21}$ parameters versus RF frequencies, as expressed in the Equation (3) and presented in Figure 14(a). The schematic shape of the input pulse is shown in Figure 15. Moreover, the average Q-factor of the full structure can be obtained from the Equation (4), as shown in Figure 14(b). The peak input power needed for 75 MV/m accelerating gradient in 0.23 m active length is 40.6 MW and the average unloaded gradient in regular cells under this condition is 94.2 MV/m. The regions for the voltage calculation of the full structure and the regular cells are illustrated in Figure 16.

$$\tau_{r\_CLIC-K} = \tau_{r\_CLIC-G} \frac{\min\left(v_{g\_CLIC-G}\right)}{\min\left(v_{g\_CLIC-K}\right)} \tag{2}$$

$$\tau_f = \frac{\partial Imag\left(ln(S_{21})\right)}{2\pi\partial f} \tag{3}$$

$$Q = \frac{2\pi f \tau_f}{-ln(|S_{21}|)} \tag{4}$$

Table 3. RF parameters of klystron-based CLIC accelerating structure.

| Parameters | Symbol | Unit | K |
|---|---|---|---|
| Frequency | f | GHz | 11.994 |
| RF phase advance per cell | Δφ | ° | 120 |
| Number of cells | $N_c$ | | 28 |
| Average Q-factor (Cu) | <Q> | | 5846 |
| Rise time | $\tau_r$ | ns | 28.6 |
| Filling time | $\tau_f$ | ns | 63.7 |
| Bunch train length | $\tau_b$ | ns | 242 |
| Pulse length | $\tau_{RF}$ | ns | 334.3 |
| Peak input power (HFSS) | $P_{in}$ | MW | 40.6 |
| Active length | L | m | 0.23 |
| Average loaded gradient | <G> | MV/m | 75 |

| | | | |
|---|---|---|---|
| Average unloaded gradient in regular cells | $<G_{un}^{Reg}>$ | MV/m | 94.2 |
| RF-to-beam efficiency | η | % | 42.5 |
| Maximum surface electric field (unloaded) | $E_s$ | MV/m | 224 |
| Maximum modified Poynting vector (unloaded) | $S_c$ | MW/mm$^2$ | 3.5 |
| Maximum pulsed surface temperature rise (unloaded) | ΔT | K | 35.8 |

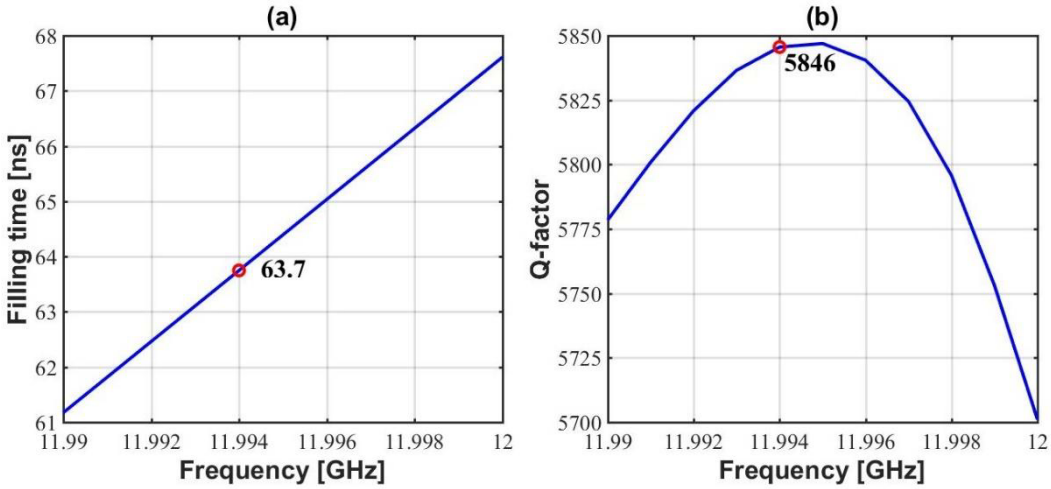


Figure 14. (a) Filling time and (b) average Q-factor calculated from $S_{21}$ parameters.

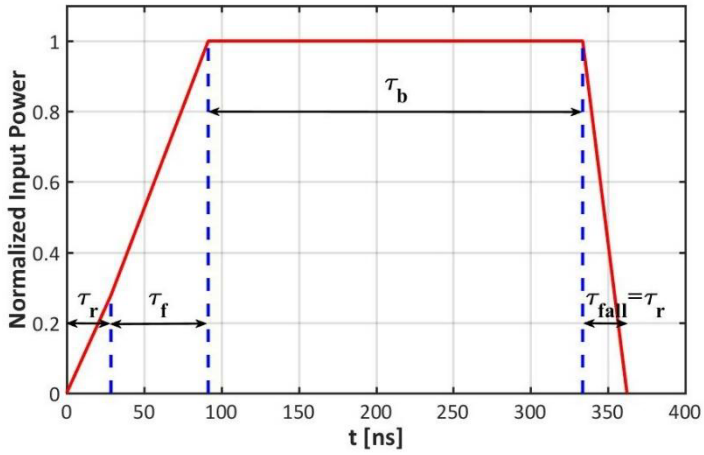


Figure 15. Schematic shape of the input pulse for CLIC-K.

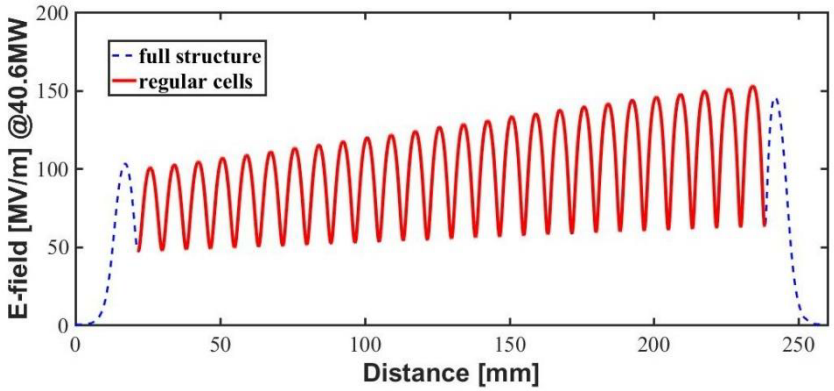


Figure 16. Electric field distribution of the full structure and of the regular cells only.

## III. Wakefield suppression

### III.1 Transverse long-range wakefield suppression

The beam dynamics study requires that the transverse wakefield potential must be below 4.75

V/pC/m/mm [29-31]. The long-range transverse wakefield of the full tapered structure was simulated by GdfidL [23]. A typical simulation took 18 hours with a mesh spacing of 0.05 mm in all three directions (a total mesh of $4.986\times10^9$) and a length of the wakefield of 16 m by using 960 CPUs. The results of the transverse wakefield potential are shown in Figure 17 for the geometry shown in Figure 10 where all damping and main waveguides are terminated with the perfectly matched layer (PML) boundary condition. The small differences between the wakefield potential on the X plane and the Y plane are due to the coupler cells. The results indicate that the envelope of the wakefield potential at the second bunch is close to 0 V/pC/m/mm.

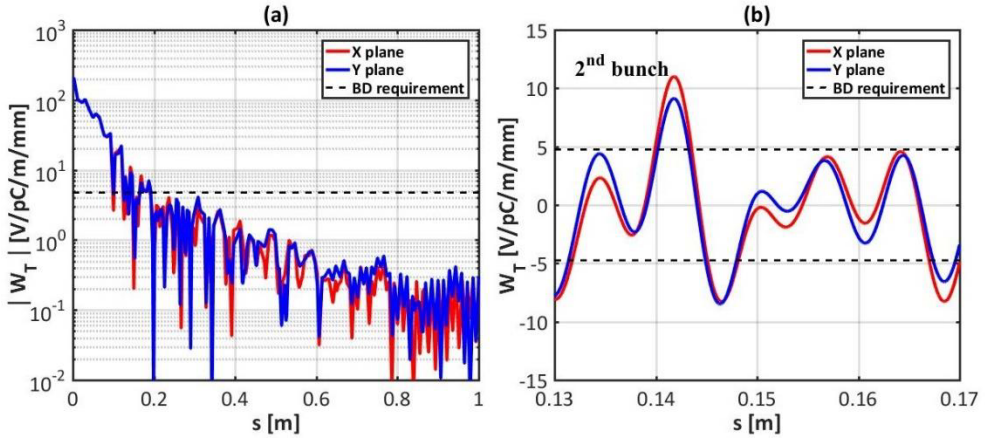


Figure 17. (a) The envelope of the long-range transverse wakefield potential. (b) Transverse wakefield potential around the position of the second bunch at 0.15 m.

The beam instability caused by long-range transverse wakefield can be described with three transverse beam jitter amplification factors: $F_c$, $F_{rms}$ and $F_{worst}$ [29]. The beam dynamics study proposed that the $F_{rms}$ should be below 2 and the $F_{worst}$ should be below 5 in order to be stable and do not have significant emittance growth along the linac. Moreover, the distribution of the transverse wakefield is related with the frequency of the wakefield dipole modes, which might be affected by the fabrication errors in the shape of the cells. These three transverse beam jitter amplification factors for the structure CLIC-K calculated with the PML boundary condition are presented in Table 4, which are better than the requirement even if the frequency of the wakefield dipole mode shifts within the range of ±1%.

Table 4. Wakefield suppression results of CLIC-K with the PML boundary condition

| Transverse beam jitter amplification factors | Ideally | | Frequency errors within ±1% | | Beam dynamics requirements |
|---|---|---|---|---|---|
| | (X) | (Y) | (X) | (Y) | |
| $F_c$ | 1.02 | 1.03 | 1.06 | 1.07 | |
| $F_{rms}$ | 1.03 | 1.09 | 1.26 | 1.34 | < 2 |
| $F_{worst}$ | 2.10 | 2.52 | 3.12 | 3.60 | < 5 |

**III.2 Design of the HOM damping loads**

To suppress the wakefield, high-order modes propagating into the four damping waveguides of the accelerating cells must be absorbed by HOM damping loads. The material of HOM loads is a silicon carbide material called “EkaSiC-P”. The properties of this material have been measured in [32]. The geometry of HOM loads designed for the updated baseline structure CLIC-G* [14] is presented in Figure 18. The tapering part from 1 × 1 mm cross-section to 5 × 5 mm is designed for broad-band absorption and low reflection from the tip. The same geometry is used for the CLIC-K as the nominal geometry.

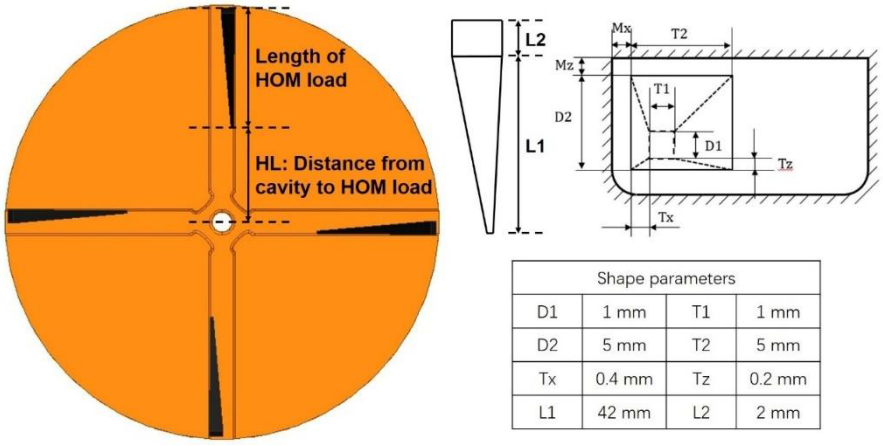


| Shape parameters | | | |
|---|---|---|---|
| D1 | 1 mm | T1 | 1 mm |
| D2 | 5 mm | T2 | 5 mm |
| Tx | 0.4 mm | Tz | 0.2 mm |
| L1 | 42 mm | L2 | 2 mm |

Figure 18. Geometry of HOM load designed for CLIC-G*.

The position of HOM loads in the damping waveguides was optimized for CLIC-K to decrease the impact on the fundamental 12 GHz mode in the accelerating cells. Ideally, when HOM loads are closer to the wall of damping waveguides, the power dissipation of fundamental mode is lower. The clearances Mx and Mz between the HOM load and waveguide wall are necessary for mechanical assembly. The final designs of Mx and Mz were both selected at 0.4 mm. The optimization of safe distance HL was conducted by HFSS, as shown in Figure 19. The distance between the center of the structure and the tip of the HOM load is 35 mm.

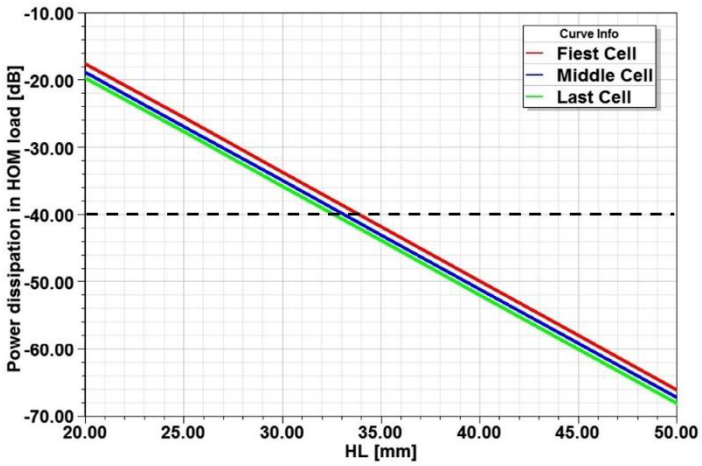


Figure 19. Power dissipation of the fundamental mode with different distance from the tip of HOM load to the center of cavity.

The transverse wakefield of the full accelerating structure with HOM loads whose geometry is shown in Figure 20 was calculated by GdfidL. The measured frequency dependence of the SiC material [32] is expressed with a dispersive N-th order Lorentz medium in GdfidL code [23]. The simulation took about 29 hours with a mesh spacing of 0.05 mm in all three directions (a total mesh of $7.666\times10^{9}$) and a length of the wakefield of 16 m by using 1280 CPUs. The results of wakefield suppression for the nominal geometry are described in Figure 21 and Table 5, which are better than the beam dynamics requirements.

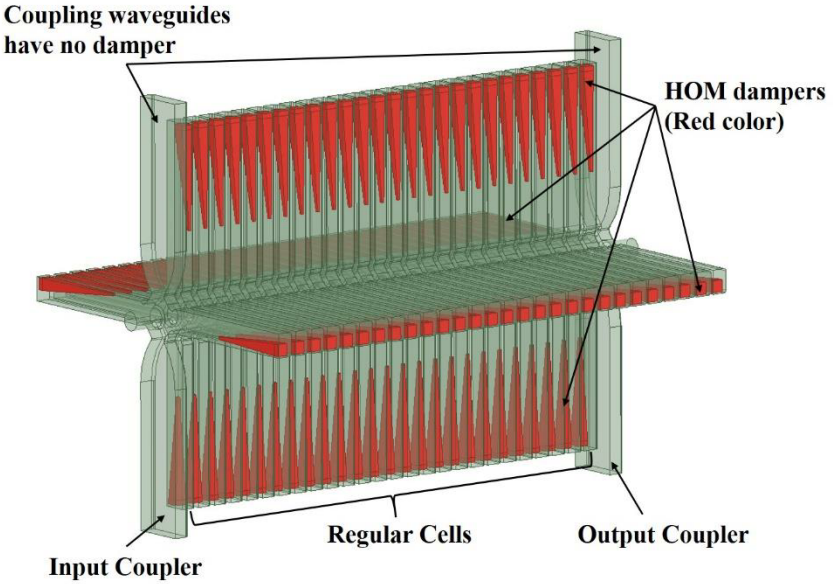


Figure 20. The view of the full accelerating structure CLIC-K with HOM loads.

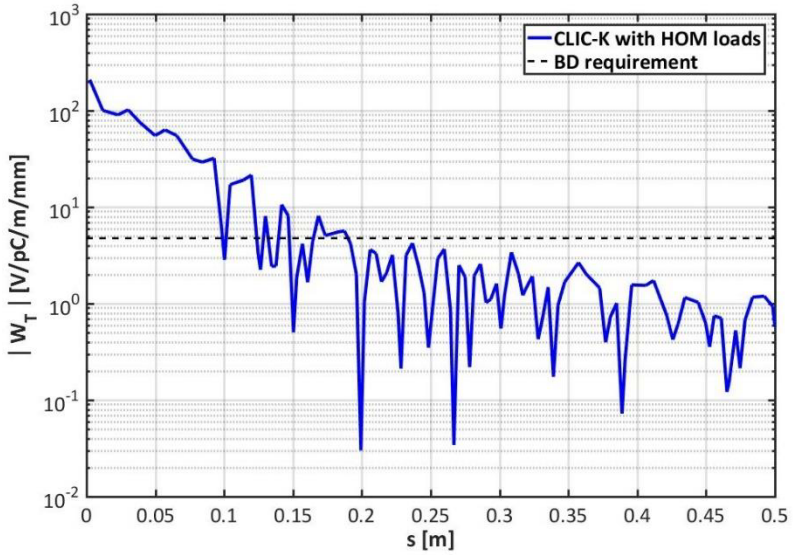


Figure 21. The envelope of transverse wakefield of CLIC-K with the HOM loads.

Table 5. Wakefield suppression results of CLIC-K with the HOM loads

| Transverse beam jitter amplification factors | Ideally | Frequency errors within ±1% | Beam dynamics requirements |
|---|---|---|---|
| $F_c$ | 1.02 | 1.06 | |
| $F_{rms}$ | 1.05 | 1.34 | < 2 |
| $F_{worst}$ | 2.19 | 3.77 | < 5 |

The properties of SiC material may vary from production batch to batch and depend on the supplier. This may result in the variation of the wakefield suppression. The sensitivity of the wakefield suppression and the SiC material properties has been simulated by using GdfidL. For the properties, ε' is the real part of permittivity and ε'' is the imaginary part of permittivity. The calculated transverse beam jitter amplification factors always meet the beam dynamics requirements when material properties vary within ±20%, as shown in Figure 22 and Figure 23.

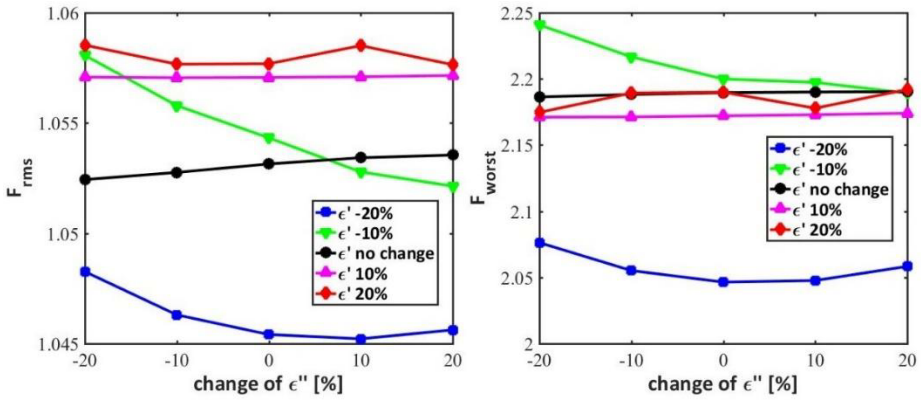


Figure 22. Wakefield suppression versus material properties of HOM loads.

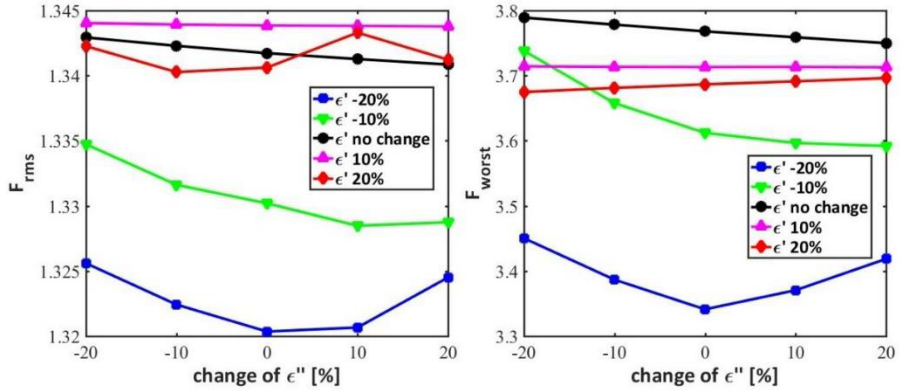


Figure 23. Wakefield suppression versus material properties of HOM loads including effect of the dipole mode frequency shift of ±1%.

Furthermore, an attempt to optimize the length of HOM loads was carried out. The dependence of the wakefield on the tapered length of HOM loads is illustrated in Figure 24. The envelope of the wakefield at the third bunch (0.3 m) is sensitive with the tapered length of HOM loads, which results in a larger $F_{worst}$ with a shorter HOM load that does not meet the beam dynamics requirement. Consequently, the geometry of the HOM loads in CLIC-K is kept same as for the optimized for 3 TeV accelerating structure CLIC-G*.

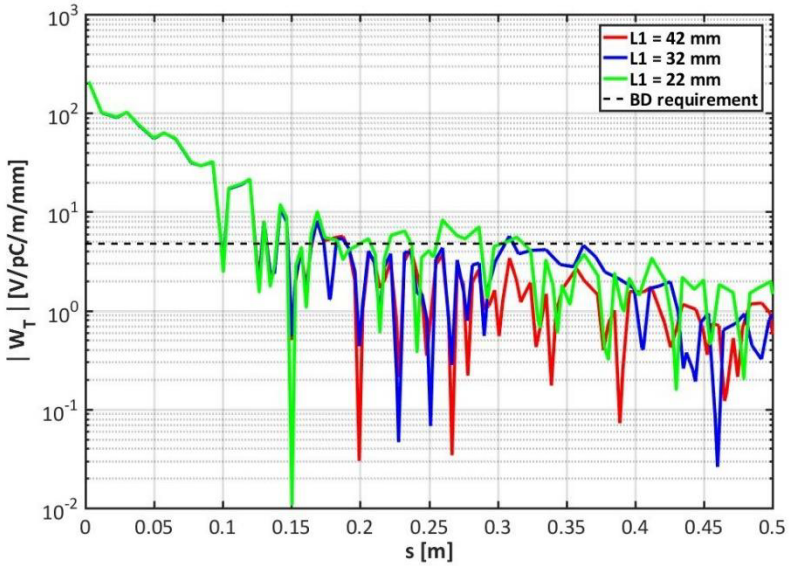


Figure 24. Wakefield suppression in CLIC-K with different tapered lengths of HOM loads

## IV. Summary

The accelerating structure named CLIC-K for the klystron-based first stage CLIC at 380 GeV was designed. It consists of 26 regular cells and 2 compact coupler cells. The average loaded accelerating gradient of this structure is 75 MV/m. The peak input power needed is 40.6 MW and the RF-to-beam efficiency is 42.5%. The results of HOM damping loads design showed good transverse wakefield suppression. The transverse wakefield potential at the second bunch was around 0 V/pC/m/mm. The tolerance study of the material properties indicated that the wakefield suppression is better than beam dynamics requirements even if the material properties changed within ±20% and the frequency of the wakefield dipole mode shifts within ±1%.

## References


[1] L. Evans, P. Bryant, LHC Machine, Journal Of Instrumentation. 3 (2008) S08001-S08001. doi:10.1088/1748-0221/3/08/s08001.

[2] International Linear Collider Technical Review Committee (ILC-TRC): Second Report, SLAC-R-606, 2003.

[3] CLIC Collaboration, CLIC Conceptual Design Report: A Multi-TeV Linear Collider Based on CLIC Technology, Report No. CERN-2012-007, 2012.

[4] CLIC and CLICdp Collaborations, Updated Baseline for a Staged Compact Linear Collider, Report No. CERN-2016-004, 2016.

[5] A. Baikov, C. Marrelli, I. Syratchev, Toward High-Power Klystrons With RF Power Conversion Efficiency on the Order of 90%, IEEE Transactions On Electron Devices. 62 (2015) 3406-3412. doi:10.1109/ted.2015.2464096.

[6] I.A. Guzilov, BAC Method of Increasing the Efficiency in Klystrons, *2014 Tenth International Vacuum Electron Sources Conference (IVESC)*, 2014.

[7] D. Schulte, *et al*., Exploration of a Klystron-powered first energy stage of CLIC, CLIC-Note-948, 2013.

[8] C. Rossi, Design Choices for the Klystron and Drive Beam Based CLIC Main Linac Modules, *The 2017 International Workshop on Future Linear Colliders (LCWS2017)*, Strasbourg, 2017.

[9] P. Wang, H. Zha, I. Syratchev, J. Shi, H. Chen, rf design of a pulse compressor with correction cavity chain for klystron-based compact linear collider, Physical Review Accelerators And Beams. 20 (2017). doi:10.1103/physrevaccelbeams.20.112001.

[10] S. Matsumoto, T. Abe, Y. Higashi, T. Higo, Y. Du, High gradient test at Nextef and high-power long-term operation of devices, Nuclear Instruments And Methods In Physics Research Section A: Accelerators, Spectrometers, Detectors And Associated Equipment. 657 (2011) 160-167. doi:10.1016/j.nima.2011.06.062.

[11] H. Zha, J. Shi, H. Chen, A. Grudiev, W. Wuensch, C. Tang et al., Choke-mode damped structure design for the Compact Linear Collider main linac, Physical Review Special Topics - Accelerators And Beams. 15 (2012). doi:10.1103/physrevstab.15.122003.

[12] A. Degiovanni, *et al.*, High-gradient test results from a CLIC prototype accelerating structure: TD26CC, CLIC-Note-1042, 2014.

[13] W. Wuensch, Advances in the understanding of the physical processes of vacuum breakdown, CLIC-Note-1025, 2014.

[14] H. Zha, A. Grudiev, Design and optimization of Compact Linear Collider main linac accelerating structure, Physical Review Accelerators And Beams. 19 (2016).

doi:10.1103/physrevaccelbeams.19.111003.

[15] W. Wuensch, *et al.*, Fabrication and high-gradient testing of an accelerating structure made from milled halves, *Proceedings of LINAC2016*, East Lansing, MI, USA, 2016.

[16] X. Wu, J. Shi, H. Chen, J. Shao, T. Abe, T. Higo et al., High-gradient breakdown studies of an X-band Compact Linear Collider prototype structure, Physical Review Accelerators And Beams. 20 (2017). doi:10.1103/physrevaccelbeams.20.052001.

[17] H. Zha, A. Grudiev, Design of the Compact Linear Collider main linac accelerating structure made from two halves, Physical Review Accelerators And Beams. 20 (2017). doi:10.1103/physrevaccelbeams.20.042001.

[18] P. Brurrows, CLIC Accelerator Status, CLIC Workshop 2018, CERN, 2018.

[19] R. Jones, Wakefield suppression in high gradient linacs for lepton linear colliders, Physical Review Special Topics - Accelerators And Beams. 12 (2009). doi:10.1103/physrevstab.12.104801.

[20] A. Grudiev, W. Wuensch, Design of an X-band Accelerating Structure for the CLIC Main Linac, *Proceeding of LINAC08*, Victoria, BC, Canada, pp. 933-935, 2008.

[21] A. Grudiev, W. Wuensch, Design of the CLIC Main Linac Accelerating Structure for CLIC Conceptual Design Report, *Proceeding of LINAC10*, Tsukuba, Japan, pp. 211-213, 2010.

[22] ANSYS HFSS, www.ansys.com/products/electronics/ansys-hfss.

[23] GdfidL, www.gdfidl.de.

[24] H. Zha, A. Latina, A. Grudiev, G. De Michele, A. Solodko, W. Wuensch et al., Beam-based measurements of long-range transverse wakefields in the Compact Linear Collider main-linac accelerating structure, Physical Review Accelerators And Beams. 19 (2016). doi:10.1103/physrevaccelbeams.19.011001.

[25] D. Pritzkau, RF pulsed heating, Report No. SLAC-Report-577, 2001.

[26] A. Grudiev, S. Calatroni, W. Wuensch, New local field quantity describing the high gradient limit of accelerating structures, Physical Review Special Topics - Accelerators And Beams. 12 (2009). doi:10.1103/physrevstab.12.102001.

[27] A. Lunin, V. Yakovlev, A. Grudiev, Analytical solutions for transient and steady state beam loading in arbitrary traveling wave accelerating structures, Physical Review Special Topics - Accelerators And Beams. 14 (2011). doi:10.1103/physrevstab.14.052001.

[28] O. Kononenko, A. Grudiev, Transient beam-loading model and compensation in Compact Linear Collider main linac, Physical Review Special Topics - Accelerators And Beams. 14 (2011). doi:10.1103/physrevstab.14.111001.

[29] D. Schulte, Multi-bunch calculations in the CLIC main linac, *Proceedings of PAC09*, Vancouver, BC, Canada, 2009.

[30] V. Khan, Detailed analysis of the long-range wakefield in the baseline design of CLIC main linac, *Proceedings of LINAC2012*, Tel-Aviv, Israel, 2012.

[31] D. Schulte, private communication.

[32] G. Michele, Wakefield simulations and measurements for the CLIC RF accelerating structure, Ecole Polytechnique Federale de Lausanne Doctoral Thesis No. 6185, 2014.